Unexpected Propeller-Like Hexakis(fluoren-2-yl)benzene Cores for Six-Arm Star-Shaped Oligofluorenes: Highly Efficient Deep-Blue Fluorescent Emitters and Good Hole-Transporting Materials

Yang Zou, Jianhua Zou, Tengling Ye, Hao Li, Chuluo Yang, Hongbin Wu,* Dongge Ma,* Jingui Qin, and Yong Cao*

Grafting six fluorene units to a benzene ring generates a new highly twisted core of hexakis(fluoren-2-yl)benzene. Based on the new core, six-arm star-shaped oligofluorenes from the first generation T1 to third generation T3 are constructed. Their thermal, photophysical, and electrochemical properties are studied, and the relationship between the structures and properties is discussed. Simple double-layer electroluminescence (EL) devices using T1–T3 as non-doped solution-processed emitters display deep-blue emissions with Commission Internationale de l'Eclairage (CIE) coordinates of (0.17, 0.08) for T1, (0.16, 0.08) for T2, and (0.16, 0.07) for T3. These devices exhibit excellent performance, with maximum current efficiency of up to 5.4 cd A^{-1}, and maximum external quantum efficiency of up to 6.8%, which is the highest efficiency for non-doped solution-processed deep-blue organic light-emitting diodes (OLEDs) based on starburst oligofluorenes, and is even comparable with other solution-processed deep-blue fluorescent OLEDs. Furthermore, T2- and T3-based devices show striking blue EL color stability independent of driving voltage. In addition, using T0–T3 as hole-transporting materials, the devices of indium tin oxide (ITO)/poly(3,4-ethylenedioxythiophene):poly(styrene sulfonic acid) (PEDOT:PSS)/T0–T3/tris(8-hydroxyquinolinato)aluminium (Alq_3)/LiF/Al achieve maximum current efficiencies of 5.51–6.62 cd A^{-1}, which are among the highest for hole-transporting materials in identical device structure.

1. Introduction

Star-shaped molecules usually comprise a central core and multiple conjugated arms as the functionalized units.[1] Extended molecular architectures, on the one hand, afford the star-shaped molecules some polymer properties, e.g., high photoluminescence quantum yields (PLQY), good thermal stabilities, and film-forming properties; on the other hand, in contrast to the polymers, which are essentially a mixture of different molecules, star-shaped molecules are still well-defined, as a consequence of which they have precise structures and physical properties, and their production is reproducible. Thus star-shaped molecules can combine the advantages of both small molecules and polymers, and so they have attracted much attention in the development of organic optoelectronics in recent years.[2–6]

Polyfluorene and its derivatives are among the most promising blue light-emitting materials due to their high photoluminescence (PL) efficiencies, wide band-gaps, good thermal stabilities and interesting morphological properties.[7–10] Their optical properties can be easily tuned by functional group substitution or copolymerization.[11–13] The solubility and film-forming ability can also facilely be improved by grafting alkyl chains on the C-9 position of the fluorene units. However, the application of the polyfluorene as a type of blue fluorescent material in organic light-emitting devices (OLEDs) is jeopardized on account of their undesirable green emissions in the process of photoirradiation, heat treatment, or device operation, which has been attributed to excimer emission arising from the aggregates in films[14–16] or generation of fluorenone defects as a result of oxidation.[17,18]

In this context, several series of star-shaped oligofluorenes with various cores (truxene, isotruxene, benzene, pyrene, triazatruxene, 4,4′,4″-tris(carbazol-9-yl)-triphenylamine, 1,3,5-tri(anthracen-10-yl) benzene, 1,4-diketo-2,3,5,6-tetraphenyl-pyrrolo[3,4-c] pyrrole) and 1 to 4 fluorene units in the arms have been synthesized,[19–30] e.g., two-dimensional architectures with three, four, or six arms,

Y. Zou, H. Li, Prof. C. Yang, Prof. J. Qin
Department of Chemistry
Hubei Key Lab on Organic and
Polymeric Optoelectronic Materials
Wuhan University
Wuhan 430072, P.R. China
E-mail: clyang@whu.edu.cn
Dr. J. Zou, Prof. H. Wu, Prof. Y. Cao
Institute of Polymer Optoelectronic Materials and Devices
State Key Laboratory of Luminescent Materials and Devices
South China University of Technology
Guangzhou 510640, P. R. China
E-mail: hbwu@scut.edu.cn
Dr. T. Ye, Prof. D. Ma
State Key Laboratory of Polymer Physics and Chemistry
Changchun Institute of Applied Chemistry
Chinese Academy of Sciences
Changchun 130022, P. R. China
E-mail: mdg1014@ciac.jl.cn

DOI: 10.1002/adfm.201202286

and three-dimensional architectures with a tetrahedral core. The bulky star-shaped architectures can render stable blue emission. Interestingly, the truxene-cored oligofluorenes with six arms exhibited significant blue-shifts in both the absorption and emission maxima and higher energy optical gaps compared to their tri-armed analogues because the steric hindrance of the ortho substituents lead to lower conjugation degree between the core and arms.[26] Aiming to develop more twisted star-shaped architectures, we initially wish to design the benzene-cored oligofluorenes, where the six oligofluorene arms are connected to the small benzene ring in ortho positions with respect to each other. Unexpected, we find that the design strategy not only creates a star-shaped oligomeric systems, but also generate a new rigid propeller-like core: hexakis(fluoren-2-yl)benzene, whose molecular structure was determined by single-crystal X-ray diffraction analysis. The thermal, photophysical, and electrochemical properties were studied, and the relationship between the structures and properties is discussed. The new star-shaped oligofluorenes have been demonstrated as good deep-blue fluorescent emitters and hole-transporting materials in OLEDs.

2. Results and Discussions

2.1. Synthesis and Characterization

The new star-shaped oligofluorenes were synthesized by convergent core-creating approach (**Scheme 1**). 1,2,3,4,5,6-hexakis(9,9-dihexyl-9*H*-fluoren-2-yl)benzene (**T0**) was synthesized via dicobaltoctacarbonyl catalyzed cyclotrimerisation of 1,2-bis(9,9-dihexyl-9*H*-fluoren-2-yl)ethyne in a high yield of 90%. The key intermediate **2Br-A0** was dexterously synthesized by using a one-pot double Sonogashira coupling reaction of trimethylsilylacetylene and 2-bromo-9,9-dihexyl-7-iodo-9*H*-fluorene, in which the trimethylsilyl group was removed automatically in the presence of 1,8-diazabicyclo[5.4.0]undec-7-ene (DBU) after the first Sonogashira coupling between the alkyne unit and C–I bond, followed by a second Sonogashira reaction. It is noteworthy that C–Br functional groups were preserved, given that its reactivity is much lower than the C–I bond in this Sonogashira reaction condition. The alkyne derivatives **A1-A3** were obtained by using Suzuki coupling reaction of **2Br-A0** with the corresponding oligofluorene boronic acid. Finally, **T1–T3** were obtained by using dicobaltoctacarbonyl catalyzed cyclotrimerisation of **A1-A3** in the yields of 52–76%. The well-defined structures and chemical purities of all intermediates and the final star-shaped macromolecules **T0–T3** were adequately verified by ^{1}H and ^{13}C NMR spectroscopy, elemental analysis, MALDI-TOF mass spectrometry (see details in the Supporting Information). The eluting curves from the gel-permeation chromatography (GPC) of **T0–T3** display symmetrical narrow peaks with polydispersities of 1.01–1.05, which indicates their monodispersity and purity (Figure S9, Supporting Information).

2.2. X-Ray Crystallography

Colorless crystals of T0 were grown by gradually evaporating the solvent of the solution of T0 in toluene. As shown in **Figure 1**, the six fluorene arms are highly twisted with respect to the benzene ring in order to alleviate the steric hindrance, which gives the molecule a propeller-like shape. Two fluorene arms of T0 orientate almost perpendicular with respect to the central benzene ring by a dihedral angle of 84.3°(C2/C2A), while the other four fluorene arms are less twisted, with dihedral angles of 60.6°(C3/C3A) and 69.0°(C1/C1A) for each pair of arms, respectively.

2.3. Thermal Properties

The good thermal stabilities of the compounds are revealed by their high decomposition temperatures (T_d, corresponding to 5% weight loss) of ca. 433 °C by thermogravimetric analysis (TGA, **Figure 2**a, **Table 1**). Distinct glass transition temperatures (T_g) can be observed at 177 (**T0**), 91 (**T1**), 103 (**T2**), and 114°C (**T3**) from differential scanning calorimetry (DSC, Figure 2b). Unexpected, **T0** shows much higher T_g than **T1–T3**. This unusual phenomenon strongly suggests that the benzene ring is not the core of these star-shaped molecules as we initially thought; instead, the propeller-like hexakis(fluoren-2-yl)benzene is the new core due to its molecular rigidity, as its crystal structure shows. This assignment can be further supported from the following aspects: i) the glass transition temperatures are enhanced with an increase of fluorene units at every arm from **T1**, **T2**, to **T3**, which is in agreement with the observations of their tri-substituted counterparts (35 °C for the 1st generation to 88 °C for the 4th generation),[19] truxene-cored oligofluorenes (tri-arm: 63 °C for the 1st generation to 116 °C for the 4th generation; six-arm: 49 °C for the 1st generation to 85 °C for the 3rd generation),[20] and the triazatruxene-cored oligofluorenes (51 °C for the 1st generation to 144 °C for the 3rd generation);[24] ii) as the wide-angle X-ray diffraction (WXRD) patterns shown (Figure S10, Supporting Information), **T0** displays several sharp peaks, indicative of its crystalline feature; in contrast, **T1–T3** exhibit similar and broad amorphous halos at ca. 2θ = 25°, which indicates that attaching the fluorene units to the propeller-like core of hexakis(fluoren-2-yl)benzene depressed the crystalline nature of the core and the linear oligofluorene arms; and, iii) DSC results reveal that **T0** has distinct melting point at 323 °C (Figure S11, Supporting Information), while **T1–T3** show glassy morphologies without obvious crystallization or melting process during the repeated scan cycles.

2.4. Photophysical Properties

The absorption spectra of **T0–T3** in toluene solution show intense π–π* absorption bands, which progressively red-shift from 314 to 365 nm with increasing chain length (**Figure 3**a). The absorption spectrum of each compound in solid state film reveals no red-shift compared to that in toluene solution (Figure 3c). **T1–T3** are highly blue emissive in both solution and solid state, with photoluminescence quantum efficiencies (Φ_{PL}) in the range of 0.82–0.92 in toluene solution using 9,10-diphenylanthracene as the reference, which are close to those of linear polyfluorenes. PL spectra are bathochromic from **T0** to **T3**, with the maximum emissions from 370 to 413 nm in solution (Figure 3b) and from 368 to 438 nm in the solid state

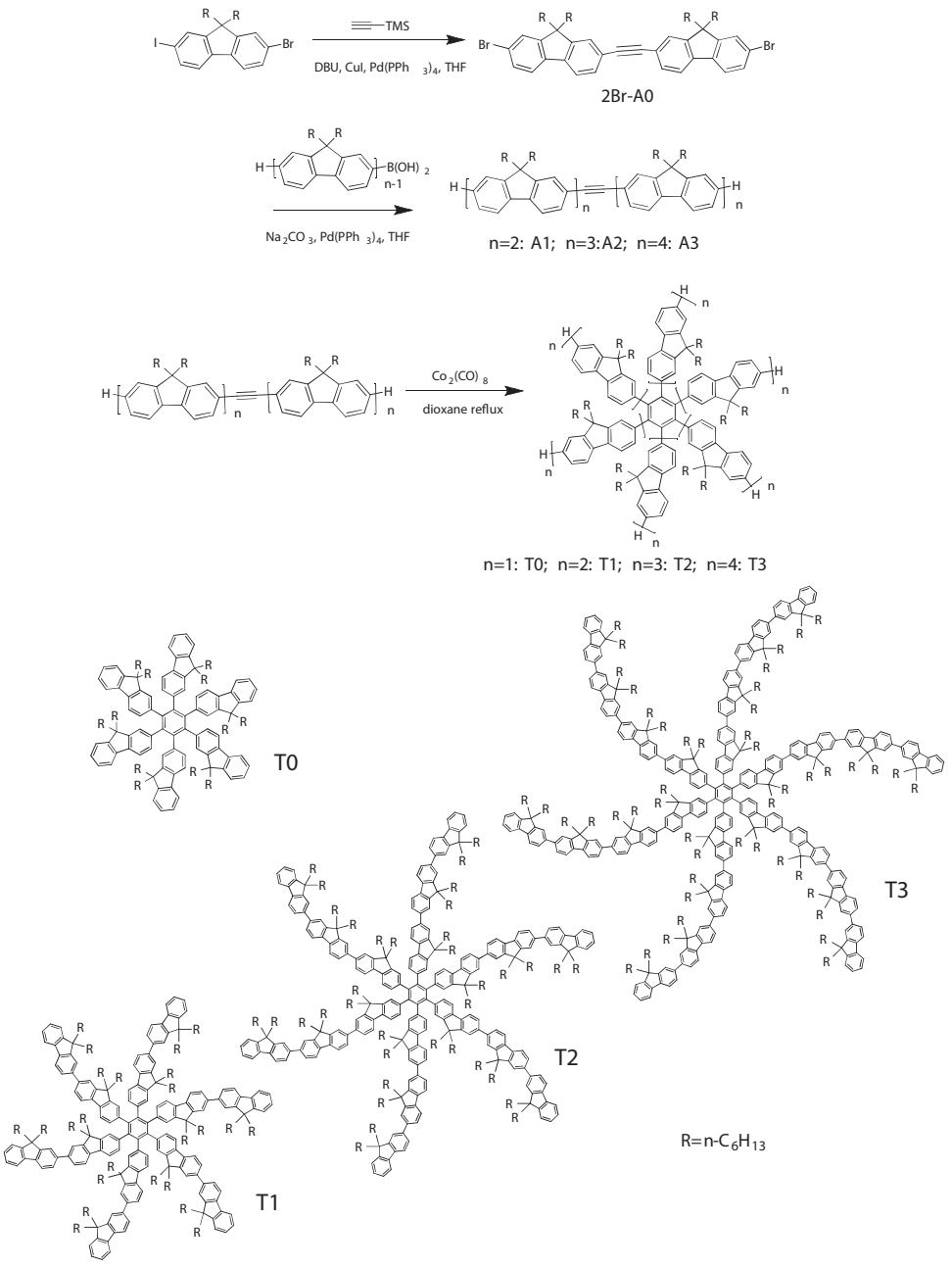

Scheme 1. Synthetic routes of **T0**–**T3** and their molecular structures.

(Figure 3d). **T0** shows only one emission peak in both solution and film due to its small π-electron conjugated system, while **T1–T3** display vibrational progression bands typical for linear oligofluorene. It is noteworthy that the relative intensity of the vibrational bands in film for **T2-T3** shows the opposite trend compared to those in solution. This can be explained by their self-absorption effects.[2]

2.5. Electrochemical Properties

Cyclic voltammetry (CV) was conducted to probe electrochemical properties of the star-shaped oligomers (**Figure 4**). **T0** shows three overlapped quasi-reversible oxidation waves at potentials of 1.36, 1.57, and 1.74 V vs. Ag/Ag^+, which can be ascribed to the through-space hole delocalization over the six fluorene units via a toroidal fashion as some hexaarybenzenes.[31,32] This is consistent with the crystal structure of **T0**: the fluorene units lie cofacially at a close distance of about 2.9 Å from each other, which allows sufficient π orbital overlapping to provide toroidal delocalization. In contrast to the oxidation behavior of **T0**, overlapped multi-reversible oxidation waves in dichloromethane are observed for **T1–T3**. With the extension of the chain length at each arm, each half-wave potential displays a negative shift and a decrease of the difference between

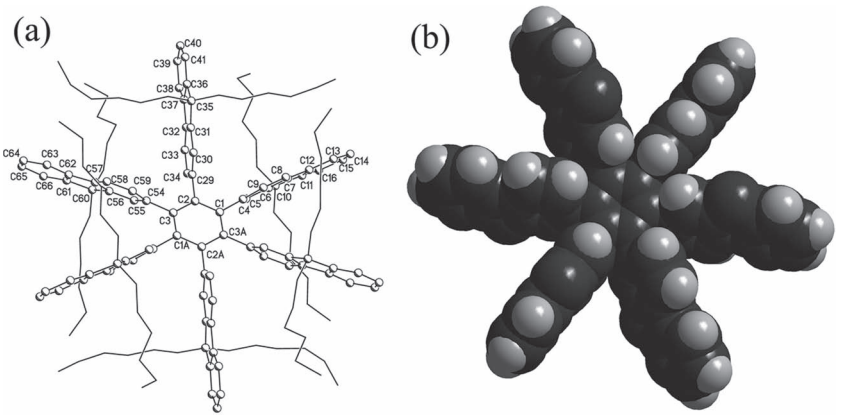

Figure 1. Crystal structures of T0: a) standard view and b) space-filling view (*n*-hexyl chains are omitted for clarity).

successive half-wave potentials [$E_{1/2}(2) - E_{1/2}(1)$]. These electrochemical behaviors of **T1–T3** are very similar to the corresponding linear oligofluorenes (dimer, trimer and tetramer),[33] indicating that each of the six oligofluorene arms is relatively independent, and no electronic interaction between the arms occurs through toroidal fashion as **T0**. We note that **T1–T3** show reversible and unvaried oxidation behavior upon repeated scanning, indicating their electrochemical stability. The thermal, photophysical, and electrochemical data of **T0–T3** are summarized in Table 1.

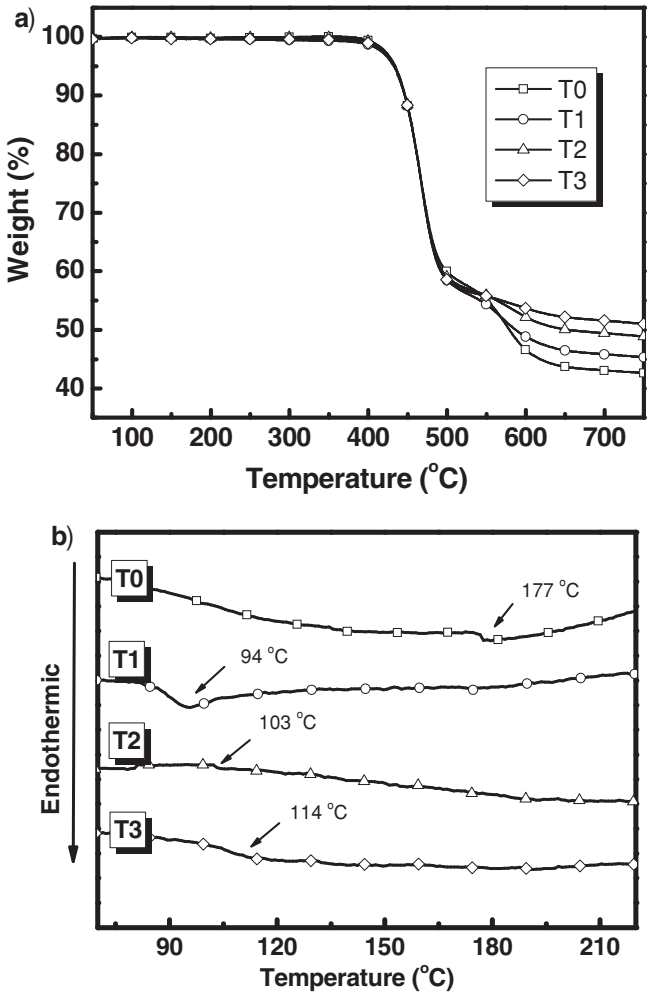

Figure 2. a) TGA thermograms of T0–T3 recorded at a heating rate of 10 °C min^{-1}. b) DSC traces of T0–T3 recorded at a heating rate of 10 °C min^{-1}.

2.6. Deep-Blue Fluorescent OLEDs

Their good solubility, high fluorescence quantum yield, and good film-forming ability enable the star-shaped oligofluorenes to be ideal candidates as solution-processable deep blue emitters in electroluminescence devices. Simple double-layer devices were fabricated with the configurations of indium tin oxide (ITO)/poly(3,4-ethylenedioxythiophene):poly(styrene sulfonic acid) (PEDOT:PSS) (50 nm)/**T1–T3** (70 nm)/1,3,5-tris(*N*-phenylbenzimidazol-2-yl)benzene (TPBI) (30 nm)/Ba (4 nm)/Al (150 nm) (**T1** for device A; **T2** for device B; **T3** for device C), in which PEDOT:PSS (poly(3,4-ethylenedioxy-thiopene):poly(styrenesulfonate)) served as hole-injecting layer, and TPBI acted as electron-transporting and hole-blocking layer. Data for all the devices are summarized in **Table 2**. **T1–T3** display deep-blue emissions with Commision Internationale de l'Eclairage (CIE) coordinates of (0.17, 0.08) for device A, (0.16, 0.08) for device B, and (0.16, 0.07) for device C (Figure 3), which are very close to the National Television System Committee standard (NTSC, 0.15, 0.07). The electroluminescence (EL) spectrum of **T1**-based device is different from its PL spectrum in film, and the green shoulder emission gradually increases with elevated driving voltages (**Figure 5**a). In contrast, the EL spectra of **T2-** and **T3**-based devices are similar to their PL spectra in film. Furthermore, the two devices exhibit striking blue EL color stability with increasing driving voltage from 4 to 11 V (Figure 5b,c). The excellent color stability can be attributed to the increasing fluorene units in each arm that may suppress the close-packing of molecules in the solid state, and resist crystallization and morphological transition-induced deterioration during the device operation.[2,24]

Figure 5d shows current efficiency and brightness versus current density curves of the devices. These devices exhibits relative high turn on voltages (6.9–8.7 V), which can be ascribed to the large hole injection barrier from PEDOT:PSS layer to the emitting layer, since the HOMO levels of **T1–T3** (from –5.65 to –5.51 eV) are remarkably lower than PEDOS:PSS (–5.1 eV). The **T1**-based device shows a maximum current efficiency ($\eta_{c,\,max}$) of 4.9 cd A^{-1}, a maximum external quantum efficiencies ($\eta_{EQE,\,max}$) of 6.1% at 2.5 mA cm^{-2}, and a maximum brightness (L_{max}) of 998 cd m^{-2}. **T2-** and **T3**-based devices exhibit better performance compared to the **T1**-based device, with $\eta_{c,\,max}$ of 5.3 and 5.4 cd A^{-1}, $\eta_{EQE,\,max}$ of 6.7% (at 9.3 mA cm^{-2}) and 6.8% (at 5.4 mA cm^{-2}), and L_{max} of 1707 and 1962 cd m^{-2}, respectively (Table 2). We note that many OLED devices based on star-shaped oligofluorenes display blue or sky-blue emission,[24,25] while few display deep-blue emission.[23,27,34,35] To the best of our knowledge,

Table 1. Thermal, photophysical, and electrochemical data of **T0–T3**.

Molecule	T_g[a] [°C]	T_d[b] [°C]	λ_{abs}[c] [nm] (toluene)	λ_{abs} [nm] (film)	λ_{PL}[c] [nm] (toluene)	λ_{PL} [nm] (film)	Φ_{PL}[d] (film)	Φ_{PL}[e] (toluene)	E_g[f] [eV]	$E_{ox}^{1/2}$[g] [V]	Ip [eV]
T0	177	434	314	317	370	365	0.34	0.42	3.67	1.45,1.65,1.83	5.72
T1	91	433	339	340	385,403sh	405,429sh	0.74	0.82	3.31	1.38, 1.76	5.65
T2	103	434	356	360	404,402sh	409,428sh	0.81	0.82	3.16	1.29, 1.55	5.56
T3	114	434	365	366	413,434sh	417,438sh	0.84	0.92	3.10	1.24, 1.42	5.51

[a]Measured on the second heating scans at 10 °C min^{-1} from 25 to 600 °C; [b]5% weight loss, measured scan rate of 10 °C min^{-1} from 20 to 800 °C under argon; [c]Measured for 1×10^{-6}M toluene solutions; [d]Measured on the quartz plate using an integrating sphere; [e] 9,10-diphenylanthracene (F_f = 0.91 in ethanol) was used as a reference; [f]Estimated from the edge of low-energy absorption edge; [g]Recorded at a scan rate of 100 mV s^{-1}; $E_{1/2}$ (ferrocene) = 0.232 V versus $AgNO_3$/Ag reference electrode.

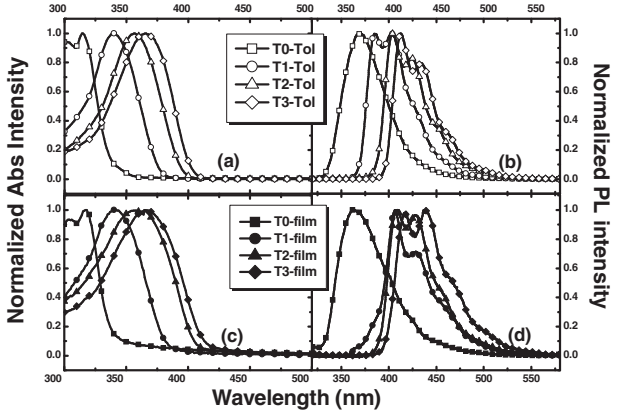

Figure 3. Absorption and emission spectra of T0–T3 in toluene (a,b) and thin film (c,d).

these efficiencies are the highest for non-doped deep-blue OLEDs based on solution-processed starburst oligofluorenes under the similar device structures, and even comparable with the state-of-the-art solution-processed deep-blue fluorescent OLEDs.[36,37] For example, the device using 4,4′,4″-tris(carbazol-9-yl)-triphenylamine cored oligofluorenes as emitters acquired

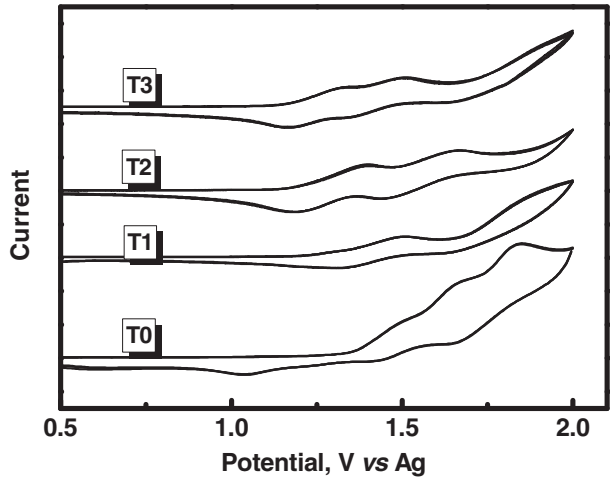

Figure 4. Cyclic voltammograms of T0–T3 in CH_2Cl_2 for oxidation.

Table 2. Electroluminescence characteristics of the devices with **T1–T3** as emitters.

Device	V_{on}[a] [V]	η_{EQE}[b] [%]	η_c[b] [cd A^{-1}]	L_{max} [cd m^{-2}]	CIE (x, y)[c]
A	8.7	6.1, 6.1	4.9, 4.9	998	(0.17, 0.08)
B	7.8	6.7, 4.6	5.3, 3.5	1707	(0.16, 0.08)
C	6.9	6.8, 6.3	5.4, 5.1	1962	(0.16, 0.07)

a)Turn-on voltage, recorded at a brightness of 1 cd m^{-2}; [b] Order of measured value: maximum, then values at 100 cd m^{-2}; [c] Recorded at 7 V.

$\eta_{c,\,max}$ of 0.47 cd A^{-1} at 100 cd m^{-2} and Commission Internationale de l'Eclairage (CIE) coordinates of (0.16, 0.07);[23] the device based on six-oligofluorene-arm triazatruxenes showed $\eta_{c,\,max}$ of 2.07 cd A^{-1} and CIE coordinates of (0.15, 0.09);[34] the device based on 1,3,5-tri(anthracen-10-yl)-benzene starburst oligofluorenes showed $\eta_{c,\,max}$ of 1.80 cd A^{-1} and CIE coordinates of (0.15, 0.10);[27] the device based on the star-shaped oligofluorenes with a planar triphenylamine core obtained $\eta_{c,\,max}$ of 3.83 cd A^{-1} and CIE coordinates of (0.16, 0.09).[35]

2.7. Hole-Transporting Properties in OLEDs

We note that the deep-blue OLED devices based on these star-shaped oligofluorenes display good performance without the additional hole transporting layer (HTL), indicating that these oligofluorenes have good hole transporting abilities. To further confirm this point, we fabricated devices of ITO/PEDOT:PSS (50 nm)/**T0–T3** (45 nm)/tris(8-hydroxyquinolinato)aluminium (Alq_3; 60 nm)/LiF (1 nm)/Al (100 nm), in which **T0–T3** was used as HTL, and Alq_3 served as light emitting layer. All these devices exhibit an exclusive emission peak at 545 nm from the Alq_3 (Figure S14, Supporting Information). These devices achieve maximum current efficiencies of 5.51–6.62 cd A^{-1}, which are substantially higher than that of the control device using *N*,*N*′-di(1-naphthyl)-*N*,*N*′-diphenyl-[1,1′-biphenyl]-4,4′-diamine (NPB) as hole-transporting layer (4.07 cd A^{-1}) (Figure S15 and Table S2, Supporting Information). To the best of our knowledge, these efficiencies are among the highest of hole-transporting materials.[38–41] As we know, the carriers balance

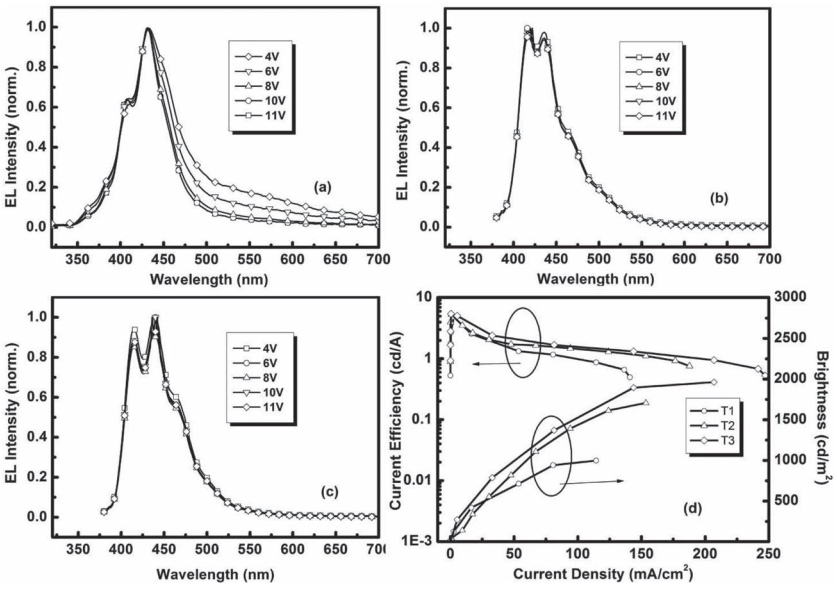

Figure 5. Normalized EL spectra of T1 (a), T2 (b), and T3 (c) at various voltages. d) Current efficiency and brightness versus current density curves for OLED devices using T1–T3 as emitters.

for an OLEDs is critical to achieve good device performance. However, the hole mobility in NPB is about 2 orders of magnitude higher than electron mobility in Alq_3, which usually makes the recombination areas near the emitting-layer/cathode interface, and thus decreases the device efficiency. As compared to NPB, the star-shaped oligofluorenes without arylamine unit may decrease the hole mobility, and result in more balance in electron and hole fluxes when they act as hole-transporting material.

3. Conclusions

In summary, we have designed and synthesized novel star-shaped oligofluorenes by a convergent core-creating approach. Grafting six fluorene units to benzene not only builds a star-shaped architecture, but also generates a new highly twisted core of hexakis(fluoren-2-yl)benzene. The relationship between their structures and thermal, photophysical, and electrochemical properties agrees with the assignment of the new propeller-like core. **T2-** and **T3-**based devices exhibit the highest efficiencies for non-doped solution-processed deep-blue OLEDs based on starburst oligofluorenes, which are even comparable with other solution-processed deep-blue fluorescent OLEDs. In addition, the new star-shaped oligofluorenes are demonstrated as good hole-transporting materials in OLEDs. We believe that more functionalized star-shaped macromolecules can be constructed on the basis of the new hexakis(fluoren-2-yl)benzene core, and this work is in progress.

4. Experimental Section

General Information: ^{1}H NMR and ^{13}C NMR spectra were measured on a Mecuyr-VX300 spectrometer. Elemental analyses of carbon, hydrogen, and nitrogen were performed on a Vario EL III microanalyzer. EI mass spectra were measured on a ZAB 3F-HF mass spectrophotometer. MALDI-TOF mass spectra were obtained on a Bruker Biflex III TOF mass spectrometer. The gel permeation chromatography (GPC) measurements were performed on a Agilent 1100 GPC with tetrahydrofuran (THF) as eluent. The calibration was based on polystyrene standards with narrow molecular weight distribution. Single-crystal X-ray diffraction data were obtained from a Bruker AXS Smart CCD diffractometer using a graphite-monochromated MoKα ($\lambda = 0.71073$Å) radiation at 77 K. The data were collected using the $\omega/2\theta$ scan mode and corrected for Lorentz and polarization effects as well as absorption during data reduction suing Shelxtl 97 software. Differential scanning calorimetry (DSC) was performed on a Netzsch DSC 200 PC unit at a heating rate of 10 °C min^{-1} from 20 to 300 °C under an argon atmosphere. The glass transition temperature (T_g) was determined from the second heating scan. Thermogravimetric analysis (TGA) was undertaken with a Netzsch STA 449C instrument. The thermal stability of the samples under a nitrogen atmosphere was determined by measuring their weight loss while heating at a rate of 10 °C min^{-1} from 25 to 600 °C. The WAXD measurements were taken on a Nanostar U X-ray scattering system using Cu Ka radiation (40 kV, 35 mA). UV-vis absorption spectra were recorded on a Shimadzu UV-2500 recording spectrophotometer. Photoluminescence (PL) spectra were recorded on a Hitachi F-4500 fluorescence spectrophotometer. Cyclic voltammetry (CV) was carried out in nitrogen-purged dichloromethane (oxidation scan) at room temperature with a CHI voltammetric analyzer. *n*-Bu_4PF_6 (0.1 M) was used as the supporting electrolyte. The conventional three-electrode configuration consists of a platinum working electrode, a platinum wire auxiliary electrode, and an Ag wire pseudoreference electrode with ferrocenium-ferrocene (Fc^+/Fc) as the internal standard. Cyclic voltammograms were obtained at a scan rate of 100 mV s^{-1}. The onset potential was determined from the intersection of two tangents drawn at the rising and background current of the cyclic voltammogram.

Device Fabrication and Measurement: For deep-blue OLEDs using **T0–T3** as emitter: patterned ITO-coated glass with a sheet resistance of 15–20 Ω square^{-1} was cleaned by a surfactant scrub followed by a wet-cleaning process inside an ultrasonic bath, beginning with deionized water, followed by acetone and isopropanol. After O_2 plasma cleaning for 4 min, PEDOT:PSS (Bayer Baytron P 4083, 50 nm) was spin-coated on the ITO substrate and then dried in a vacuum oven at 80 °C overnight. The emissive layer (EML) was coated on the top of PEDOT:PSS by spin-coating from a solution of chlorobenzene, and then annealed at 100 °C for 10 min to remove the solvent residue. The thickness of the EML was about 70 nm. Finally, an electron-transporting layer of TPBI (30 nm) and a cathode that was composed of Ba (4 nm) and an Al (150 nm) layer were evaporated with a shadow mask at a base pressure of 3×10^{-4} Pa. The thickness of the evaporated cathode was monitored by a quartz crystal thickness/ratio monitor (model: STM-100/MF, Sycon). The overlapping area between the cathode and the anode defined a pixel size of 19 mm^2. Except for the deposition of the PEDOT layers, all of the fabrication processes were carried out inside a controlled atmosphere of a nitrogen dry-box (Vacuum Atmosphere Co.) that contained less than 10 ppm oxygen and moisture. The current density–luminance–voltage characteristics were measured by using a Keithley 2400 source measurement unit and a calibrated silicon photodiode. The forward-viewing luminance was calibrated by a spectrophotometer (SpectraScan PR-705, Photo Research) and the forward-viewing LE was calculated accordingly. Herein, the luminance and LE values were for the forward-viewing direction only. The external quantum efficiency of EL was collected

by measuring the total light output in all directions in an integrating sphere (IS-080, Labsphere). The EL spectra were collected on a PR-705 photometer. For green OLEDs using **T0–T3** as HTL: the ITO-coated glass substrates were cleaned with special detergent and deionized water. After cleaning, the substrates were baked at 120 °C for 20 min followed by O_2 plasma treatment. 50 nm of PEDOT:PSS (Bayer Baytron P 4083), which was used as a hole-injection layer at the anode interface, was spin-coated on the ITO substrate and then dried in a vacuum oven at 80 °C overnight. **T0–T3** were spin-coated from the solution in chlorobenzene onto the layer of PEDOT:PSS. After baking at 120 °C for 30 min, the emitting layer of Alq_3 was deposited by thermal evaporation at a base pressure less than 1×10^{-4} Pa. Finally, a 1 nm thick layer of LiF and a 100 nm thick film Al were thermally deposited as a cathode under vacuum. If needed, NPB was also deposited by thermal evaporation under the same conditions. The thickness of the films deposited by thermal evaporation was monitored by the crystal thickness meter and the thickness of spin-coated films was measured by the terrace detector. The active areas of the devices were 16 mm^2, determined by the cross-breadth between the cathode and the ITO. The EL spectra were measured using a JY SPEX CCD3000 detector. Steady current–luminance–voltage was measured by a Keithley 2400 with silicon photodiode. All tests were performed under air atmosphere and at room temperature.

Materials: Unless otherwise indicated, all starting materials were obtained from commercial suppliers and were used without further purification, including trimethylsilylethynylene, CuI, tetrakis(triphenylphosphine) palladium ($Pd(PPh_3)_4$), potassium carbonate, and 1,8-diazabicyclo[5.4.0] undec-7-ene (DBU). Solvents for synthesis were purified by routine procedure and distilled under dry argon prior to use. 1,2-bis(9,9-dihexyl-9H-fluoren-2-yl)ethyne[42], 2-bromo-9,9-dihexyl-7-iodo-9H-fluorene,[43] and oligofluorene boronic acids[34] were prepared according to the literature.

1,2-Bis(7-bromo-9,9-dihexyl-9H-fluoren-2-yl)ethyne (2Br-A0): To a mixture of 2-bromo-9,9-dihexyl-7-iodo-9*H*-fluorene (8.1 g, 15 mmol), CuI (0.15 g, 0.75 mmol) and $Pd(PPh_3)_4$ (0.315 g, 0.45 mmol) was added degassed THF (75 mL) and DBU (13.5 mL). The mixture was stirred for 5 min under argon, then ethynyltrimethylsilane (1.05 mL, 7.4 mmol) and water (0.2 mL, 11 mmol) was quickly added. The mixture was sealed up and stirred for 24 h at room temperature. Then the resulting mixture was poured into ice-water and extracted with chloroform. The combined organic layer was washed with dilute HCl and then water, dried over Na_2SO_4. Then removed the solvent under reduced pressure, the residue was then purified with a silicon gel column using chloroform/hexane (1:10, v/v) as the eluent to obtain the desired product as a white powder (5.4 g, 85%). ^{1}H NMR (300 MHz, $CDCl_3$, δ): 7.66 (d, 2H, J = 7.8 Hz), 7.57-7.52 (m, 6H), 7.47-7.45 (m, 4H), 1.95 (t, 8H, J = 5.7 Hz), 1.16-1.06 (m, 24H), 0.78 (t, 12H, J = 6.9 Hz), 0.61-0.60 (m, 8H); ^{13}C NMR (75 MHz, $CDCl_3$, δ): 150.77, 147.98, 137.85, 136.99, 128.29, 127.67, 128.29, 127.67, 123.72, 123.47, 119.54, 119.13, 118.87, 117.32, 88.22, 53.02, 37.91, 29.06, 27.21, 21.25, 20.14, 11.54. MS (EI, m/z): $[M]^+$ Calcd. for $C_{52}H_{64}Br_2$: 848.3; found: 848.4. Anal. calcd. for $C_{52}H_{64}Br_2$: C 73.57, H 7.60; found: C 73.19, H 7.86.

General Procedure for Bis(oligofluorene)ethyne **A1**, **A2**, *and* **A3**: To a mixture of 1,2-bis(7-bromo-9,9-dihexyl-9*H*-fluoren-2-yl)ethyne (**2Br-A0)** (1.7 g, 2 mmol) and corresponding oligofluorene boronic acid (2.5 equiv, 5 mmol), $Pd(PPh_3)_4$ (0.15 g, 0.2 mmol), and K_2CO_3 (1.38 g, 10 mmol) was added degassed THF (20 mL) and water (5 mL). The mixture was refluxed under argon for 24 h. The resulting mixture was poured into water and extracted with chloroform. The combined organic layer was washed with water and dried over Na_2SO_4. Then the solvent was removed under reduced pressure, the residue was purified with a silicon gel column using chloroform/hexane (v/v) 1:10 for **A1**, 1:5 for **A2**, 1:3 for **A3** as the eluent to obtain the product.

A1: Yield 75%, colorless solid. ^{1}H NMR (300 MHz, $CDCl_3$, δ): 7.79-7.71 (m, 6H), 7.65-7.57 (m, 16H), 7.35-7.32 (m, 4H), 2.03 (m, 16H), 1.07 (m, 48H), 0.76-0.75 (m, 40H). ^{13}C NMR (75 MHz, $CDCl_3$, δ): 152.07, 151.76, 151.36, 151.26, 141.34, 141.29, 141.01, 140.73, 140.58, 139.92, 130.98, 127.31, 127.08, 126.53, 126.34, 123.19, 121.84, 121.64, 120.51, 120.19, 120.01, 91.02, 55.58, 55.44, 40.75, 40.65, 31.80, 31.75, 29.97, 24.05, 22.89, 22.84, 14.32, 14.27. MS (MALDI-TOF, m/z): $[M]^+$ Calcd. for $C_{102}H_{130}$: 1356.02; found: 1355.7. Anal. calcd. for $C_{102}H_{130}$: C 90.34, H 9.66; found: C 90.11, H 9.49.

A2: Yield 72%, colorless solid. ^{1}H NMR (300 MHz, $CDCl_3$, δ): 7.81-7.58 (m,32 H), 7.33-7.31 (m, 6H), 2.06 (m, 24H), 1.09 (m, 72H), 0.75 (m, 60H). ^{13}C NMR (75 MHz, $CDCl_3$, δ): 154.52, 154.18, 153.71, 143.75, 143.06, 142.63, 142.40, 133.45, 129.52, 128.91, 125.61, 124.17, 122.69, 122.45, 93.49, 58.04, 43.11, 34.18, 32.41, 26.53, 25.28, 16.73. MS (MALDI-TOF, m/z): $[M]^+$ Calcd. for $C_{152}H_{194}$: 2020.5; found: 2019.8. Anal. calcd. for $C_{152}H_{194}$: C 90.33, H 9.67; found: C 89.93, H 9.96.

A3: Yield 69%, colorless solid. ^{1}H NMR (300 MHz, $CDCl_3$, δ): 7.85-7.60 (m, 44H), 7.36-7.32 (m, 6H), 2.11 (m, 32H), 1.13 (m, 96H), 0.79-0.78 (m, 60H). ^{13}C NMR (75 MHz, $CDCl_3$, δ): 154.74, 154.39, 154.04, 153.93, 143.99, 143.72, 143.42, 143.27, 142.90, 142.62, 133.66, 129.72, 129.11, 125.83, 124.44, 122.90, 122.65, 93.69, 58.25, 58.09, 43.29, 34.38, 32.59, 26.745, 25.47, 16.94. MS (MALDI-TOF, m/z): $[M]^+$ Calcd. for $C_{202}H_{258}$: 2686.0; found: 2686.3. Anal. calcd. for $C_{202}H_{258}$: C 90.32, H 9.68; found: C 90.08, H 9.65.

*General Procedure for **T0**, **T1**, **T2**, and **T3***: To a mixture of bis(oligofluorene) ethyne (3 mmol) and dicobaltoctacarbonyl (52 mg, 0.15 mmol) was added 60 mL of degassed 1,4-dioxane. The solution was refluxed under argon for 24 h. The resulting mixture was poured into water; the solid was collected by filtration. The crude product was purified by column chromatography using hexane for **T0**, chloroform/hexane (v/v) 1:5 for **T1**, 1:3 for **T2**, and 1:1 for **T3** as the eluent to obtain the final product.

T0: Yield 90%, colorless crystals. ^{1}H NMR (300 MHz, $CDCl_3$, δ): 7.09 (m, 30H), 6.97 (d, 6H, J = 8.2 Hz), 6.82 (d, 6H, J = 7.8 Hz), 1.72 (m, 24H), 1.07 (m, 24H), 0.89 (m, 48H), 0.75 (t, 36H, J = 6 Hz), 0.22 (m, 24H). ^{13}C NMR (75 MHz, $CDCl_3$, δ): 150.72, 149.38, 141.27, 141.19, 139.91, 138.43, 129.41, 126.46, 122.50, 119.77, 118.03, 54.76, 40.75, 31.70, 30.10, 23.57, 23.00, 14.26. MS (MALDI-TOF, m/z): $[M]^+$: Calcd. for $C_{156}H_{198}$: 2072.6. Found: 2072.7. Anal. calcd. for $C_{156}H_{198}$: C 90.37, H 9.63. Found: C 90.05, H 9.44.

T1: Yield 76%, white solid. ^{1}H NMR (300 MHz, $CDCl_3$, δ): 7.71-7.69 (m, 12H), 7.52-7.50 (m, 6H), 7.46-7.41 (m, 24H), 7.31-7.29 (m, 24H), 7.18 (s, 4H), 7.08 (d, 4H, J = 7.2 Hz), 6.92 (d, 4H, J = 7.8 Hz), 1.96-1.83 (m, 60H), 1.15-1.02 (m, 144H), 0.80-0.67 (m, 96H), 0.40 (m, 12H). ^{13}C NMR (75 MHz, $CDCl_3$, δ): 151.55, 151.23, 149.87, 141.41, 141.07, 140.45, 140.28, 140.03, 138.25, 129.70, 127.10, 126.97, 126.69, 126.16, 125.99, 123.12, 121.71, 121.35, 119.96, 119.87, 118.19, 55.31, 55.00, 40.79, 40.52, 31.80, 31.65, 30.17, 29.86, 23.96, 23.75, 23.07, 22.75, 14.36, 14.20. MS (MALDI-TOF, m/z): $[M]^+$ Calcd. for $C_{306}H_{390}$: 4068.1; found: 4065.8. Anal. calcd. for $C_{306}H_{390}$: C 90.34, H 9.66; found: C 90.15, H 9.40.

T2: Yield 68%, white solid. ^{1}H NMR (300 MHz, $CDCl_3$, δ): 7.78-7.64 (m, 24H), 7.60-7.51 (m, 36H), 7.44 (m, 18H), 7.34-7.32 (m, 18H), 7.21 (s, 6H), 7.10 (d, 6H, J = 6.6 Hz), 6.96 (d, 6H, J = 7.2 Hz), 2.02-1.85 (m, 60H), 1.07 (m, 202H), 0.82-0.73 (m, 172H), 0.42 (m, 24H). ^{13}C NMR (75 MHz, $CDCl_3$, δ): 152.06, 151.94, 151.74, 151.29, 149.95, 141.47, 141.10, 140.82, 140.60, 140.31, 140.06, 138.33, 129.80, 127.26, 127.08, 126.33, 123.19, 121.72, 120.16, 120.00, 118.29, 55.51, 55.45, 55.08, 40.68, 40.55, 31.89, 31.77, 31.68, 30.25, 29.99, 29.89, 24.08, 23.83, 23.14, 22.85, 22.79, 14.44, 14.28. MS (MALDI-TOF, m/z): $[M]^+$ Calcd. for $C_{456}H_{582}$: 6063.6; found: 6062.0. Anal. calcd. for $C_{456}H_{582}$: C 90.33, H 9.67; found: C 90.15; H 9.81.

T3: Yield 52%, white solid. ^{1}H NMR (300 MHz, $CDCl_3$, δ): 7.82-7.73 (m, 36H), 7.67-7.63 (m, 46H), 7.58-7.46 (m, 28H), 7.36-7.33 (m, 22H), 7.22 (s, 6H), 7.11 (d, 6H, J = 6.6 Hz), 6.96 (d, 6H, J = 7.2 Hz), 2.04-1.87 (m, 96H), 1.28-1.09 (m, 292H), 0.84-0.75 (m, 216H), 0.432 (m, 20H). ^{13}C NMR (75 MHz, $CDCl_3$, δ): 152.07, 151.95, 151.75, 151.29, 141.09, 140.83, 140.63, 140.28, 127.08, 126.42, 126.33, 123.19, 121.80, 120.23, 120.00, 55.60, 55.51, 55.45, 40.66, 31.87, 31.73, 30.24, 29.98, 29.94, 24.08, 23.14, 22.83, 14.43, 14.29. MS (MALDI-TOF, m/z): $[M]^+$ Calcd. for $C_{606}H_{774}$: 8057.1; found: 8057.0. Anal. calcd. for $C_{606}H_{774}$: C 90.32, H 9.68; found: C 89.94, H 9.59.

Supporting Information

Supporting Information is available from the Wiley Online Library or from the author.

Acknowledgements

C.Y. thanks the National Science Fund for Distinguished Young Scholars of China (No. 51125013), the National Basic Research Program of China (973 Program 2009CB623602), and the National Natural Science Foundation of China (90922020); H.W. thanks the National Natural Science Foundation of China (61177022); J.Z. thanks the China Postdoctoral Science Foundation (201104352) for financial support.

Received: August 13, 2012
Revised: September 20, 2012
Published online: November 2, 2012

[1] A. L. Kanibolotsky, I. F. Perepichka, P. J. Skabara, *Chem. Soc. Rev.* **2010**, *39*, 2695.
[2] W. Y. Lai, R. Xia, Q. Y. He, P. A. Levermore, W. Huang, D. D. C. Bradley, *Adv. Mater.* **2009**, *21*, 355.
[3] R. Xia, W. Y. Lai, P. A. Levermore, W. Huang, D. D. C. Bradley, *Adv. Funct. Mater.* **2009**, *19*, 2844.
[4] W. W. H. Wong, T. B. Singh, D. Vak, W. Pisula, C. Yan, X. Feng, E. L. Williams, K. L. Chan, Q. Mao, D. J. Jones, C.-Q. Ma, K. Müllen, P. Bäuerle, A. B. Holmes, *Adv. Funct. Mater.* **2010**, *20*, 927.
[5] L. Chen, P. Li, Y. Cheng, Z. Xie, L. Wang, X. Jing, F. Wang, *Adv. Mater.* **2011**, *23*, 2986.
[6] K. Y. Pu, K. Li, B. Liu, *Adv. Mater.* **2010**, *22*, 643.
[7] A. W. Grice, D. D. C. Bradley, M. T. Bernius, M. Inbasekaran, W. W. Wu, E. P. Woo, *Appl. Phys. Lett.* **1998**, *73*, 629.
[8] M. Kreyenschmidt, G. Klaerner, T. Fuhrer, J. Ashenhurst, S. Karg, W. D. Chen, V. Y. Lee, J. C. Scott, R. D. Miller, *Macromolecules* **1998**, *31*, 1099.
[9] F. Huang, Y. Zhang, M. S. Liu, Y. J. Cheng, A. K. Y. Jen, *Adv. Funct. Mater.* **2007**, *17*, 3808.
[10] Q. Zhao, S. J. Liu, W. Huang, *Macromol. Chem. Phys.* **2009**, *210*, 1580.
[11] M.-C. Hung, J. L. Liao, S. A. Chen, S. H. Chen, A. C. Su, *J. Am. Chem. Soc.* **2005**, *127*, 14576.
[12] B. Liu, W. L. Yu, Y. H. Lai, W. Huang, *Chem. Mater.* **2001**, *13*, 1984.
[13] S. Gong, C. Yang, J. Qin, *Chem. Soc. Rev.* **2012**, *41*, 4797.
[14] J. Huber, K. Müllen, J. Salbeck, H. Schenk, U. Scherf, T. Stehlin, R. Stern, *Acta Polym.* **1994**, *45*, 244.
[15] U. Lemmer, S. Heun, R. F. Mahrt, U. Scherf, M. Hopmeier, U. Siegner, E. O. Göbel, K. Müllen, H. Bässler, *Chem. Phys. Lett.* **1995**, *240*, 373.
[16] S. A. Jenekhe, J. A. Osaheni, *Science* **1994**, *265*, 765.
[17] E. J. W. List, R. Guentner, P. Scanducci de Freitas, U. Scherf, *Adv. Mater.* **2002**, *14*, 374.
[18] S. Y. Cho, A. C. Grimsdale, D. J. Jones, S. E. Watkins, A. B. Holmes, *J. Am. Chem. Soc.* **2007**, *129*, 11910.
[19] X. H. Zhou, J. C. Yan, J. Pei, *Org. Lett.* **2003**, *5*, 3543.
[20] A. L. Kanibolotsky, R. Berridge, P. J. Skabara, I. F. Perepichka, D. D. C. Bradley, M. Koeberg, *J. Am. Chem. Soc.* **2004**, *126*, 13695.
[21] W. Y. Lai, Q. Q. Chen, Q. Y. He, Q. L. Fan, W. Huang, *Chem. Commun.* **2006**, 1959.
[22] J. S. Yang, Y. R. Lee, J. L. Yan, M. C. Lu, *Org. Lett.* **2006**, *8*, 5813.
[23] Q. D. Liu, J. Lu, J. Ding, M. Day, Y. Tao, P. Barrios, J. Stupak, K. Chan, J. Li, Y. Chi, *Adv. Funct. Mater.* **2007**, *17*, 1028.
[24] W. Y. Lai, Q. Y. He, R. Zhu, Q. Q. Chen, W. Huang, *Adv. Funct. Mater.* **2008**, *18*, 265.
[25] F. Liu, W. Y. Lai, C. Tang, H. B. Wu, Q. Q. Chen, B. Peng, W. Wei, W. Huang, Y. Cao, *Macromol. Rapid Commun.* **2008**, *29*, 659.
[26] W. Y. Lai, R. Xia, D. D. C. Bradley, W. Huang, *Chem. Eur. J.* **2010**, *16*, 8471.
[27] H. Huang, Q. Fu, S. Zhuang, Y. Liu, L. Wang, J. Chen, D. Ma, C. Yang, *J. Phys. Chem. C* **2011**, *115*, 4872.
[28] J. Luo, Y. Zhou, Z. Q. Niu, Q. F. Zhou, Y. Ma, J. Pei, *J. Am. Chem. Soc.* **2007**, *129*, 1131.
[29] S. Jeeva, S. C. Moratti, *Synthesis* **2007**, *2007*, 3323.
[30] A. L. Kanibolotsky, F. Vilela, J. C. Forgie, S. E. T. Elmasly, P. J. Skabara, K. Zhang, B. Tieke, J. McGurk, C. R. Belton, P. N. Stavrinou, D. D. C. Bradley, *Adv. Mater.* **2011**, *23*, 2093.
[31] C. Lambert, *Angew. Chem. Int. Ed.* **2005**, *44*, 7337.
[32] S. V. Rosokha, I. S. Neretin, D. Sun, J. K. Kochi, *J. Am. Chem. Soc.* **2006**, *128*, 9394.
[33] C. Chi, G. Wegner, *Macromol. Rapid Commun.* **2005**, *26*, 1532.
[34] W. Y. Lai, R. Zhu, Q. L. Fan, L. T. Hou, Y. Cao, W. Huang, *Macromolecules* **2006**, *39*, 3707.
[35] C. Liu, Y. Li, Y. Zhang, C. Yang, H. Wu, J. Qin, Y. Cao, *Chem. Eur. J.* **2012**, *18*, 6928.
[36] C. G. Zhen, Z. K. Chen, Q.-D. Liu, Y. F. Dai, R. Y. C. Shin, S. Y. Chang, J. Kieffer, *Adv. Mater.* **2009**, *21*, 2425.
[37] L. Wang, Y. Jiang, J. Luo, Y. Zhou, J. Zhou, J. Wang, J. Pei, Y. Cao, *Adv. Mater.* **2009**, *21*, 4854.
[38] J. Li, C. Ma, J. Tang, C. S. Lee, S. Lee, *Chem. Mater.* **2005**, *17*, 615.
[39] Z. Jiang, T. Ye, C. Yang, D. Yang, M. Zhu, C. Zhong, J. Qin, D. Ma, *Chem. Mater.* **2010**, *23*, 771.
[40] O. Usluer, S. Demic, D. A. M. Egbe, E. Birckner, C. Tozlu, A. Pivrikas, A. M. Ramil, N. S. Sariciftci, *Adv. Funct. Mater.* **2010**, *20*, 4152.
[41] Z. Jiang, Z. Liu, C. Yang, C. Zhong, J. Qin, G. Yu, Y. Liu, *Adv. Funct. Mater.* **2009**,*19*, 3987.
[42] S. H. Lee, T. Nakamura, T. Tsutsui, *Org. Lett.* **2001**, *3*, 2005.
[43] V. Promarak, A. Punkvuang, T. Sudyoadsuk, S. Jungsuttiwong, S. Saengsuwan, T. Keawin, K. Sirithip, *Tetrahedron* **2007**, *63*, 8881.